Jake J. Abbott*
Allison M. Okamura
Department of Mechanical Engineering
Johns Hopkins University
Baltimore, MD 21218

Pseudo-admittance Bilateral Telemanipulation with Guidance Virtual Fixtures

Abstract

Pseudo-admittance is introduced as a novel bilateral telemanipulation system that is designed to mimic proportional-velocity admittance control on systems where the master is an impedance-type robot. The controller generalizes to systems with slave robots of the impedance or admittance type. Pseudo-admittance uses a proxy with admittance dynamics combined with direct force feedback from the slave, resulting in unique properties that mimic admittance control and exhibit tremor attenuation and quasi-static transparency. Pseudo-admittance control has potential benefits for tasks that require better-than-human levels of precision, as well as with systems that are typically run under rate control. The controller can also be modified to include virtual fixtures that provide guidance during task execution, while leaving ultimate control of the system with the operator. Guidance virtual fixtures could be used as macros that increase both speed and precision on structured tasks that require direct human control. The properties of the system are verified through simulations and experiments.

KEY WORDS—telerobotics, teleoperation, admittance control, rate control, virtual mechanism, proxy, motion scaling

1. Introduction

Bilateral telemanipulation refers to systems in which a human operator manipulates a master robotic device, and a slave robotic device emulates the behavior of the master, with some form of haptic feedback to the operator. In this paper, we present a novel bilateral telemanipulation scheme that we call Pseudo-admittance. Admittance control, where the controlled velocity of the robot is proportional to the applied force, is typically implemented on admittance-type robots, which can be modeled as nonbackdrivable, with velocity-source actuators (the nonbackdrivability typically comes from large friction and gearing in electromechanical systems, and from valves and fluid incompressibility in hydraulic systems, as is typical of industrial robots). Pseudo-admittance control mimics admittance control on telemanipulation systems with impedance-type masters. Robots of the impedance type are backdrivable, with low inertia, low friction, and force-source actuators, as is typical of haptic devices. Since Pseudo-admittance control does not require admittance-type hardware, it can be overlayed on existing impedance-type telemanipulators designed for transparency. The controller can then be turned on and off as desired. Our method generalizes to systems with impedance- or admittance-type slaves.

Pseudo-admittance bilateral telemanipulation is a proxy-based control system (Zilles and Salisbury 1995; Ruspini et al. 1997); other work has considered telemanipulation schemes that make use of dynamic proxies (Micaelli et al. 1998; Turro et al. 2001; Abbott and Okamura 2003; Mitra and Niemeyer 2004). Our novel scheme works as follows: a proxy exists in software, the slave robot servos to the proxy, the master servos to the slave, the measured slave/environment force is scaled and fed directly to the master (in addition to the force due to the master servo), and the proxy moves as a function of the error between the master and the slave positions. The algorithm is described in detail in Sections 2.1 and 2.3.

When commanding the slave robot through free space, Pseudo-admittance control results in a slave velocity that is roughly linearly proportional to the user's applied force. When the robot contacts an environment, the controller feels roughly like force control. The control system is designed to have

The International Journal of Robotics Research
Vol. 26, No. 8, August 2007, pp. 865–884
DOI: 10.1177/0278364907080425

Figure 11 appear in color online: http://ijr.sagepub.com

* J. J. Abbott is now with the Institute of Robotics and Intelligent Systems, ETH Zurich, 8092 Zurich, Switzerland. jabbott@ethz.ch

asymmetries that provide desirable steady-hand characteristics, in that high-frequency movements of the master are attenuated at the slave, but still allow for high-fidelity force feedback from the slave to the master. Pseudo-admittance control also exhibits quasi-static transparency. That is, the system has static equilibrium points if and only if there is perfect (scaled) position correspondence between the master and the slave, and the (scaled) slave/environment interaction force is perfectly reflected to the user. In addition, this property is closely approximated when the system is moving slowly. The system can generate large slave/environment interaction forces, regardless of controller gains. The stability of the controller is discussed in Sections 2.2 and 2.4. Pseudo-admittance is designed for tasks that require better-that-human levels of precision. We are particularly interested in applications in robot-assisted surgery, where procedures are often difficult to perform due to lack of sensory feedback to the user.

1.1. Position, Rate, and Pseudo-admittance Control

Figure 1 depicts how Pseudo-admittance control compares to traditional position and rate control. Pseudo-admittance control has potential benefits for systems that are traditionally run under rate control (where the velocity of the slave manipulator corresponds to the position of the master), such as heavy hydraulic equipment (Parker et al. 1993; Lawrence et al. 1995). Rate control is typically desirable when either the workspace of the slave is much larger than the workspace of the master, or the slave device has restrictive velocity saturation. If position control is used on systems with significant workspace scaling, hand tremor and other undesirable movements of the user are amplified at the slave. Rate control also has potential benefits even without scaling, if the precision required at the slave manipulator is beyond the limits of the human user, since the slave can be commanded to move very slowly. In recent years, researchers have worked towards providing force feedback on telemanipulators under rate control. It is not obvious how best to add force feedback to rate-controlled systems, due to the kinematic differences between the master and the slave, and this is still an active area of research. Methods to create transparent rate-controlled bilateral telemanipulation are discussed by Mobasser and Hashtrudi-Zaad (Mobasser and Hashtrudi-Zaad 2004), where *transparency* is defined as accurately presenting the environment's impedance to the human user. An alternative is Naturally Transitioning Rate-to-Force Control (Williams et al. 1999), which acts like rate control when the slave is moving in free space, and acts like force control when the slave is constrained by an environment.

However, positioning tasks are most intuitively accomplished using position control (Kim et al. 1987; Zhai and Milgram 1993), and consequently, researchers have worked toward correcting the deficiencies in position control, as an alternative to rate control. Casals et al. (2003) introduce a

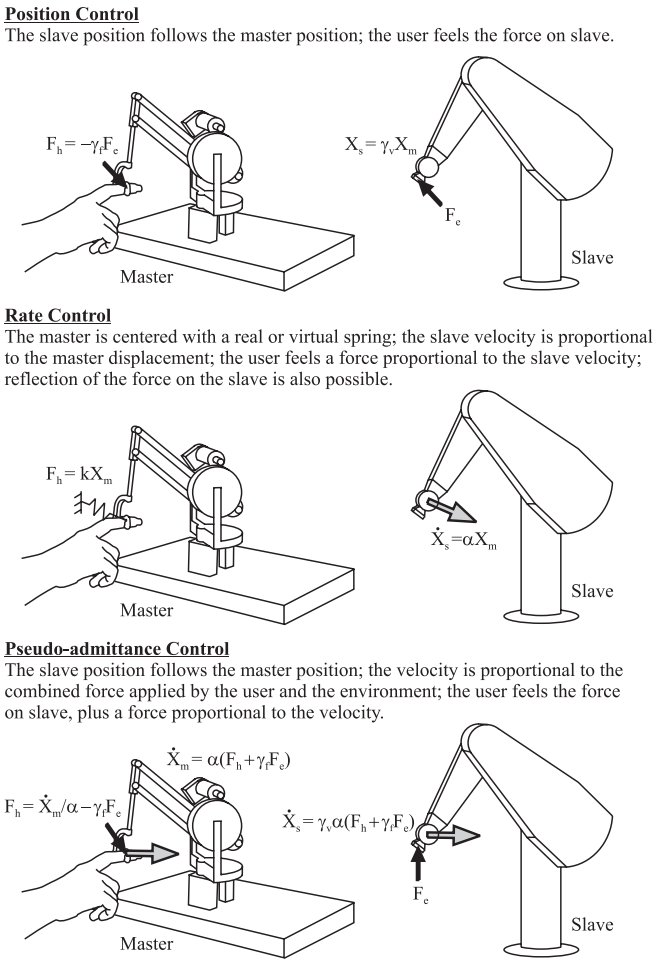

Fig. 1. Comparison of Pseudo-admittance control to traditional position and rate control. All telemanipulation schemes are idealized. X_m and X_s are the master and slave positions, respectively. α is an admittance constant, k is a spring constant, and γ_v and γ_f are velocity and force scaling gains, respectively. The master and slave are not drawn to scale.

workspace-deformation method that increases precision at key locations in the workspace, at the expense of reducing precision elsewhere. Abbott and Okamura (2003) and Kontz and Book (2003) present methods that provide alternatives to rate control by making use of a proxy to retain some of the benefits of rate control. These two systems are, roughly speaking, impedance-type masters implementing admittance-type controllers, through the use of a "virtual coupling" (Colgate et al. 1995; Adams and Hannaford 1999). Some of the noted benefits of this type of system are desirable "steady-hand" properties that attenuate undesirable user movements at the slave (Abbott and Okamura 2003), and the ability to switch between position and rate control (Kontz and Book 2003). Pseudo-admittance control also provides a novel alternative to

rate control that retains some of the benefits of traditional position control. Like (Williams et al. 1999), Pseudo-admittance control is also "naturally transitioning," in that it requires no controller switching event in the transition between free and constrained motion.

1.2. Guidance Virtual Fixtures

The structure of the Pseudo-admittance controller also lends itself to the implementation of guidance virtual fixtures (GVFs). GVFs assist the user in moving the slave manipulator along desired paths or surfaces (Figure 2). GVFs have been implemented on passive cooperative robotic systems (where the human and robot simultaneously act on a single end-effector) known as Cobots (Moore et al. 2003). These GVFs act passively in the sense that they are only able to restrict, and not generate, motion. It is also possible to implement similar GFVs using active admittance-type systems. Bettini et al. (2004) implemented GVFs on the Johns Hopkins University Steady-Hand Robot, which is an admittance-type cooperative manipulator. Extension of these GVFs to telemanipulators where both the master and slave manipulators are admittance-type devices is fairly straightforward. In this paper, we extend these GVFs to telemanipulators with impedance-type masters. When implementing GVFs via Pseudo-admittance control, the user retains ultimate control to move the slave anywhere in the workspace. The user also experiences quasi-static transparency in both the constrained and the unconstrained directions. This property is unique among previous implementations of GVFs. A detailed review of virtual fixtures (by that name and others) can be found in Abbott (2005) and Abbott et al. (2007).

One of the potential uses of GVFs under Pseudo-admittance control is as task-specific macros that would allow a user to quickly and safely conduct structured tasks. Some research has investigated autonomous macros for surgical tasks, but GVFs provide a higher level of operator control. For example, a virtual ruler could be used to move the slave in a straight line or on a flat plane. GVFs could also potentially assist in suturing tasks for minimally invasive surgery (Kang and Wen 2000). For bone drilling tasks, to avoid damage to the bit, the drill should only be moved axially once the drilling begins (Esen et al. 2003); GVFs could be used in this application. GVFs could also be used with remote-center-of-motion robotic movements for needle placement (Boctor et al. 2005). Another GVF could then be used to assist in the needle insertion after the alignment. In short, GVFs have potential benefits for tasks exhibiting structure.

This paper is structured as follows. We present Pseudo-admittance bilateral telemanipulation with both impedance- and admittance-type slaves in Section 2, and detail its defining characteristics and stability properties. In Section 3, we explain how GVFs can be incorporated into the Pseudo-admittance controller, and discuss their features. We then verify the properties of Pseudo-admittance control with and without GVFs through experiments and simulations in Section 4. Throughout this paper, scalar quantities are represented by lower-case letters, and matrix quantities (including vectors) are represented by upper-case letters.

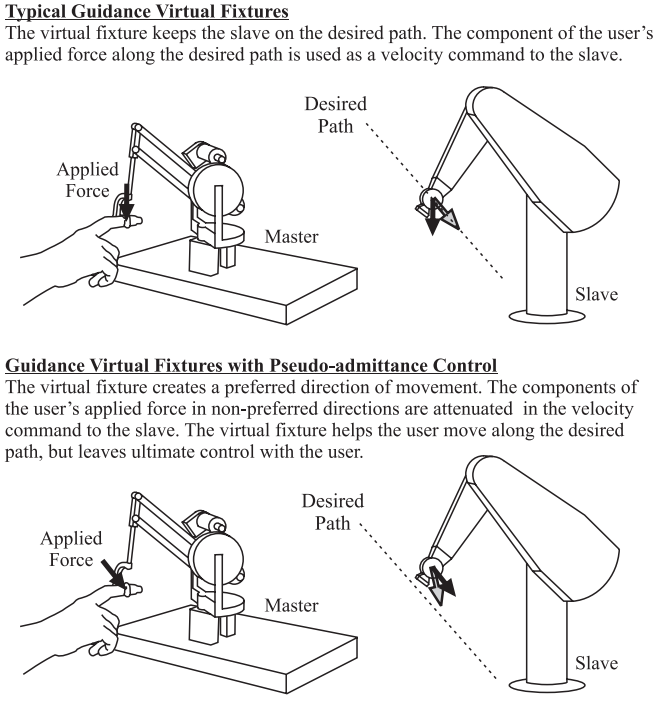

Fig. 2. Guidance virtual fixtures assist the user in moving the manipulator along desired paths or surfaces. The velocity commanded to the proxy is indicated by a gray arrow. The master and slave are not drawn to scale.

2. Pseudo-admittance Bilateral Telemanipulation

Pseudo-admittance control is designed to mimic the following admittance control system:

$$\dot{X}_m = \alpha(F_h + \gamma_f F_e) \quad (1)$$

$$\dot{X}_s = \gamma_v \alpha(F_h + \gamma_f F_e) \quad (2)$$

where $\dot{X}_m$ and $\dot{X}_s$ are the master and slave velocities, respectively, F_h and F_e are the applied human and slave/environment forces, respectively, γ_v is a velocity (or workspace) scaling gain, γ_f is a force scaling gain, and α is a user-defined admittance gain. Descriptions of the variables used in the Pseudo-admittance controller can be found in Table 1. This type of

Table 1. Definition of variables used in the Pseudo-admittance controller. For variables containing a subscript i, $i = m$ for the master, $i = s$ for the slave, and $i = p$ for the proxy.

Variable	Definition
X_i	Position
$\dot{X}_i$	Velocity
F_h	Force applied by human on master
F_e	Force applied by environment on slave
α	Admittance gain
γ_f	Gain scaling force from slave to master
γ_v	Gain scaling velocity from master to slave
k_{pi}	Proportional servo gain
k_{di}	Derivative servo gain
F_{ci}	Force generated by controller
F_{ai}	Force applied by actuators
F_{PDm}	Component of F_h due to master servo
M_{xi}	Cartesian inertia matrix
$\hat{M}_{xi}$	Estimate of Cartesian inertia matrix
Q_{xi}	Cartesian Coriolis/centrifugal/gravity vector

admittance control law, also known as proportional-velocity control, has previously been explored with the Johns Hopkins University Steady Hand Robot (Roy and Whitcomb 2002), a human–machine cooperative system, and was shown to have desirable steady-hand properties. In addition, this control law exhibits the desirable property of being unconditionally stable (Hashtrudi-Zaad and Salcudean 2001), meaning it will stably interact with any passive human and environment, for any choice of the three positive system gains. The admittance control of (1) and (2) can be accomplished directly if both the master and slave devices are of the admittance type. However, many telemanipulators have haptic master devices of the impedance type. Pseudo-admittance allows us to apply the advantageous properties of admittance control to these systems.

2.1. Control Algorithm for Impedance-type Slave

The master and slave devices we consider are assumed to be serial-link robots with dynamics

$$M_i(\Theta_i)\ddot{\Theta}_i + Q_i(\Theta_i, \dot{\Theta}_i) = \Upsilon_{ai} + J_i^T(\Theta_i)F \tag{3}$$

where Θ_i is the vector of joint variables, M_i is the positive-definite inertia matrix, Q_i is the vector containing Coriolis and centrifugal terms, as well as gravity effects and joint friction, Υ_{ai} is the vector of joint actuator forces/torques, and J_i is the robot's Jacobian, where $i = (m, s)$ for the master and slave robots. F is the force vector that is externally applied to the robot end effector, expressed in the same frame as the Jacobian. For the master device, $F = F_h$, the force applied by the human; for the slave, $F = F_e$, the environmental force.

The dynamics of the end-effector of a serial-link manipulator change as a function of the position in the workspace. Pseudo-admittance control is a Cartesian controller, so in order to obtain the uniform desired response of the slave throughout the workspace, we implement a linearizing and decoupling control law (details in the Appendix). Using the linearizing and decoupling controller, we assume a decoupled unit-mass system governed by

$$\ddot{X}_i = F_{ci} + M_{xi}^{-1}(\Theta_i)F \tag{4}$$

where X_i is the Cartesian position of the robot, M_{xi} is the Cartesian inertia matrix, and F_{ci} is the Cartesian controller force vector. It is also possible to implement the Pseudo-admittance controller without implementing the linearizing and decoupling control law on the master or the slave, but that will not be pursued here.

We command the slave to servo to the proxy, using proportional control with velocity feedback:

$$F_{cs} = k_{ps}(\gamma_v X_p - X_s) - k_{ds}\dot{X}_s \tag{5}$$

X_p is the position of the proxy, defined in the master workspace, and k_{ps} and k_{ds} are the positive proportional and derivative control gains.

We command the master to servo to the slave using proportional-derivative (PD) control. In addition, we feed forward a scaled version of the measured environmental force:

$$\begin{aligned} F_{cm} &= k_{pm}(X_s/\gamma_v - X_m) + k_{dm}(\dot{X}_s/\gamma_v - \dot{X}_m) \\ &+ M_{xm}^{-1}(\Theta_m)\gamma_f F_e. \end{aligned} \tag{6}$$

The appearance of the Cartesian inertia matrix in (6) is an artefact of the linearizing and decoupling control law (see Appendix). The actual actuator force applied to the master end-effector is

$$\begin{aligned} F_{am} &= M_{xm}(\Theta_m)\left(k_{pm}(X_s/\gamma_v - X_m)\right. \\ &+ \left. k_{dm}(\dot{X}_s/\gamma_v - \dot{X}_m)\right) + \gamma_f F_e \\ &+ Q_{xm}(\Theta_m, \dot{\Theta}_m). \end{aligned} \tag{7}$$

The proxy moves with the programmed dynamics

$$\dot{X}_p = \alpha F_{PDm} \tag{8}$$

where α is the positive admittance gain, and F_{PDm} is the component of the user's applied force due to the master's PD servo controller:

$$\begin{aligned} F_{PDm} &= \hat{M}_{xm}(\Theta_m)(k_{pm}(X_m - X_s/\gamma_v) \\ &+ k_{dm}(\dot{X}_m - \dot{X}_s/\gamma_v)) \end{aligned} \tag{9}$$

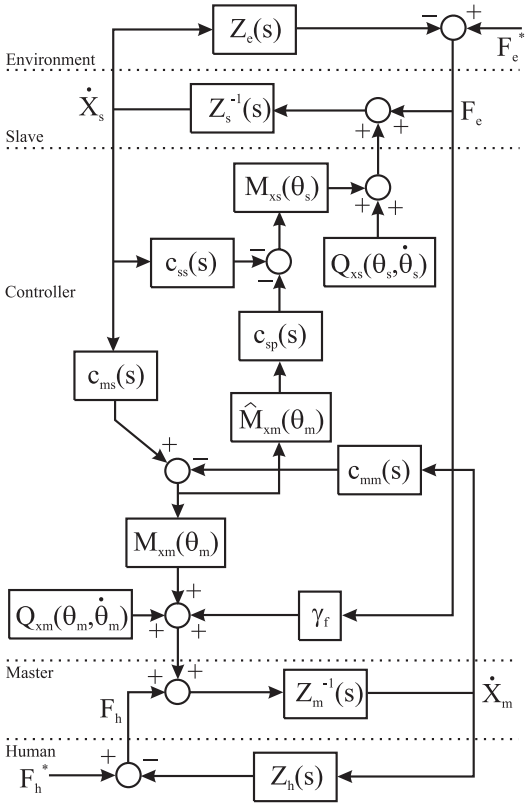

Fig. 3. Block diagram of Pseudo-admittance bilateral telemanipulation with an impedance-type slave. A linearizing and decoupling controller is also implemented (see Appendix).

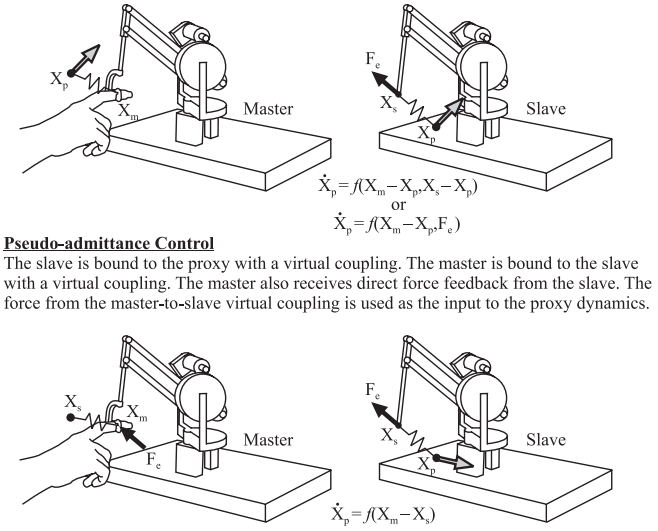

Fig. 4. Pseudo-admittance control with an impedance-type slave compared to traditional schemes using virtual couplings to a proxy with admittance dynamics.

where $\hat{M}_{xm}$ is a slowly updated estimate of M_{xm}. We assume that our estimate of M_{xm} is accurate and updated continuously for the purposes of the linearizing and decoupling controller, but in the proxy dynamics it is updated at a rate that is slow relative to the other system dynamics for the purposes of ensuring stability, as discussed in detail in Section 2.2.

Figure 3 shows a block diagram of Pseudo-admittance control with a linearizing and decoupling controller and an impedance-type slave. The individual controllers are:

$$c_{ms}(s) = \frac{1}{\gamma_v}\left(\frac{k_{dm}s + k_{pm}}{s}\right) \quad (10)$$

$$c_{mm}(s) = \frac{k_{dm}s + k_{pm}}{s} \quad (11)$$

$$c_{sp}(s) = \frac{\gamma_v \alpha k_{ps}}{s} \quad (12)$$

$$c_{ss}(s) = \frac{k_{ds}s + k_{ps}}{s}. \quad (13)$$

The human and environment impedances are given by Z_h and Z_e, respectively. The effective Cartesian master and slave device impedances are represented by Z_m and Z_s, respectively. They are nonlinear and vary across the workspace in general.

Pseudo-admittance has elements in common with prior work that uses proxies and virtual couplings to implement admittance-type virtual environments with impedance-type devices. However, there are differences between Pseudo-admittance and typical similar implementations. Figure 4 compares Pseudo-admittance with an impedance-type slave to an implementation of (1) and (2) using virtual couplings to a proxy. Unlike with standard implementations, there is no direct mechanical analogy of Pseudo-admittance control; this leads to the novel behavior exhibited by the controller.

For the purpose of system analysis, we will be particularly interested in two error variables: the position error between the slave and the proxy ($E_s = X_s - \gamma_v X_p$), and the position error between the master and slave ($E_m = X_s/\gamma_v - X_m$). The system dynamic equations, in terms of these error variables, are given by:

$$\ddot{X}_m = k_{pm}E_m + k_{dm}\dot{E}_m + M_{xm}^{-1}(\Theta_m)(F_h + \gamma_f F_e) \quad (14)$$

$$\ddot{X}_s = -k_{ps}E_s - k_{ds}\dot{X}_s + M_{xs}^{-1}(\Theta_s)F_e \quad (15)$$

$$\dot{X}_p = -\alpha \hat{M}_{xm}(\Theta_m)(k_{pm}E_m + k_{dm}\dot{E}_m). \quad (16)$$

For the purpose of analysis, we are interested in expressing our system with respect to the variables $\dot{E}_m$, E_m, $\dot{X}_s$, E_s, and X_p. The system written in this state-space form is given as:

$$\begin{bmatrix} \ddot{E}_m \\ \dot{E}_m \\ \ddot{X}_s \\ \dot{E}_s \\ \dot{X}_p \end{bmatrix} = \begin{bmatrix} -k_{dm}I & -k_{pm}I & -k_{ds}I/\gamma_v & -k_{ps}I/\gamma_v & 0 \\ I & 0 & 0 & 0 & 0 \\ 0 & 0 & -k_{ds}I & -k_{ps}I & 0 \\ \alpha k_{dm}\hat{M}_{xm}(\Theta_m) & \alpha k_{pm}\hat{M}_{xm}(\Theta_m) & I & 0 & 0 \\ -\alpha k_{dm}\hat{M}_{xm}(\Theta_m) & -\alpha k_{pm}\hat{M}_{xm}(\Theta_m) & 0 & 0 & 0 \end{bmatrix} \begin{bmatrix} \dot{E}_m \\ E_m \\ \dot{X}_s \\ E_s \\ X_p \end{bmatrix} + \begin{bmatrix} -M_{xm}^{-1}(\Theta_m) & M_{xs}^{-1}(\Theta_s)/\gamma_v - \gamma_f M_{xm}^{-1}(\Theta_m) \\ 0 & 0 \\ 0 & M_{xs}^{-1}(\Theta_s) \\ 0 & 0 \\ 0 & 0 \end{bmatrix} \begin{bmatrix} F_h \\ F_e \end{bmatrix}. \tag{17}$$

2.2. Stability for Impedance-type Slave

To analyze the stability of (17), we must first begin by defining what *stability* means for our system. From an arbitrary initial condition, we would like the unforced system ($F_h = F_e = 0$) to come to rest ($\dot{X}_m, \dot{X}_s, \dot{X}_p \to 0$) with no position error between the master and the slave ($E_m \to 0$). We cannot characterize the stability of our system by the stability of some equilibrium state vector. For our system, the position of the proxy X_p (and consequently the master and slave position) should move around the workspace in an unbounded fashion; there is no zero position to which we would like the unforced system to return.

The block-triangular structure of the state matrix in (17) allows us to consider the stability of the error system (consisting of just the first four states) independently from X_p. We would like this system (when unforced) to have a stable equilibrium at the zero state vector. We would also like this system to be bounded-input/bounded-output (BIBO) stable; that is, bounded external forces should lead to bounded master and slave velocities and bounded position errors in the system. From (17), it is clear that a bounded $\dot{E}_m$ and E_m result in a bounded $\dot{X}_p$. While X_p does not explicitly enter into the error dynamics, it does affect the value of the Cartesian inertia matrices.

With $E = [\dot{E}_m^T \; E_m^T \; \dot{X}_s^T \; E_s^T]^T$ and $U = [F_h^T \; F_e^T]^T$, (17) can be rewritten as

$$\begin{bmatrix} \dot{E} \\ \dot{X}_p \end{bmatrix} = \begin{bmatrix} A(t) & 0 \\ G(t) & 0 \end{bmatrix} \begin{bmatrix} E \\ X_p \end{bmatrix} + \begin{bmatrix} B(t) \\ 0 \end{bmatrix} U.$$

Then stability, as described above, can be characterized by considering the stability of

$$\dot{E} = A(t)E + B(t)U. \tag{18}$$

We begin by considering the unforced system $\dot{E}(t) = A(t)E(t)$. If we consider the $A(t)$ matrix when $\alpha = 0$:

$$A_0 = \begin{bmatrix} -k_{dm}I & -k_{pm}I & -k_{ds}I/\gamma_v & -k_{ps}I/\gamma_v \\ I & 0 & 0 & 0 \\ 0 & 0 & -k_{ds}I & -k_{ps}I \\ 0 & 0 & I & 0 \end{bmatrix} \tag{19}$$

it is clear from the block-triangular structure of A_0 that the system eigenvalues are those of the master and slave servo controllers. A_0 is also linear time-invariant (LTI). The PD gains can be chosen to place the eigenvalues where desired; if they are chosen such that A_0 is Hurwitz, the system $\dot{E}(t) = A_0E(t)$ will be *uniformly exponentially stable* (Rugh 1996). We have chosen to neglect sample-and-hold effects, but in practice, the local master and slave servo gains will be limited by sampling and quantization effects. We assume here that those local controllers are suitably designed to be robust to sampled-data effects.

We now return to the original $A(t)$ matrix. The matrix $M_{xm}(\Theta_m)$ is bounded, assuming that the robot is bounded away from any singular configurations. From the continuity of matrix eigenvalues, we know that $A(t)$ will be Hurwitz for sufficiently small α. We can rewrite $A(t)$ as:

$$A(t) = A_0 + \tilde{A}(t)$$

where A_0 is defined in (19) and

$$\tilde{A}(t) = \begin{bmatrix} 0 & 0 & 0 & 0 \\ 0 & 0 & 0 & 0 \\ 0 & 0 & 0 & 0 \\ \alpha k_{dm}\hat{M}_{xm}(t) & \alpha k_{pm}\hat{M}_{xm}(t) & 0 & 0 \end{bmatrix}. \tag{20}$$

Because A_0 is uniformly exponentially stable and bounded, there exists a positive constant β such that $\dot{E}(t) = A(t)E(t)$ is uniformly exponentially stable if $\|\tilde{A}(t)\| \leq \beta \ \forall t$ (Rugh 1996). For a given master device, this is essentially a small-gain result limiting α.

To develop a more constructive stability condition, we consider the system where the matrix $\hat{M}_{xm}(\Theta_m)$ is updated at a constant rate with a period of τ seconds. We assume that α has been chosen small enough such that all of the LTI systems that may potentially be switched to are exponentially stable. For each LTI A_i matrix in this set, the system response is

$$E(t) = e^{A_i t}E(0). \tag{21}$$

We are interested in the evolution of the state vector from one switching event to the next:

$$E(k+1) = e^{A_i \tau}E(k). \tag{22}$$

By making use of an induced matrix norm (Horn and Johnson 1985), we find that:

$$\|E(k+1)\| \leq \|e^{A_i \tau}\|\|E(k)\|. \tag{23}$$

We can ensure that the norm of the state vector exponentially decreases to zero at the switching times by requiring

$$\|e^{A_i \tau}\| < 1 \quad \forall A_i. \tag{24}$$

Also note that the induced matrix norm is equal to the maximum singular value of the matrix ($\bar{\sigma}(\cdot) = \|\cdot\|$). We know that for all Hurwitz A_i, $\|e^{A_i \tau}\| \to 0$ as $\tau \to \infty$. If we implement an update period of τ such that $\|e^{A_i t}\| < 1 \ \forall A_i, \forall t \geq \tau$, we can be assured that the norm of the state vector, sampled at the switches, exponentially decreases to zero. A practical implementation of this condition is a numerical search for τ after selecting all other system parameters: we select an initial τ, numerically calculate the matrix norm in (24) at many locations around the workspace, find the maximum value that this norm obtains, and then raise or lower τ appropriately and iterate until (24) is satisfied.

Each of the LTI A_i systems are uniformly exponentially stable (Rugh 1996); that is, there exist positive constants ψ_i and λ_i such that for any t_0 and $E(t_0)$:

$$\|E(t)\| \leq \psi_i e^{-\lambda_i (t-t_0)}\|E(t_0)\|. \tag{25}$$

The exponential convergence of the state vector norm at the switching times (described above) can also be bounded by a continuous-time exponential decay:

$$\|E(t)\| \leq e^{-\tilde{\lambda} t}\|E(t_0)\| \tag{26}$$

where

$$\tilde{\lambda} = -\frac{\ln(\max_i \|e^{A_i \tau}\|)}{\tau} \tag{27}$$

for the specific value of τ chosen. Synthesizing these two facts, the unforced system $\dot{E}(t) = A(t)E(t)$ is found to be uniformly exponentially stable:

$$\|E(t)\| \leq \overline{\psi} e^{-\underline{\lambda}(t-t_0)}\|E(t_0)\| \tag{28}$$

where $\overline{\psi} \geq \max\{\psi_i\}$ and $\underline{\lambda} \leq \min\{\{\lambda_i\}, \tilde{\lambda}\}$.

We now return to the forced system, and consider BIBO stability. The output we are concerned with is the entire state vector $E(t)$. Assuming that both the master and slave robots are bounded away from any singular configurations, we know that $B(t)$ is bounded. That is, there exists a finite constant β such that $\|B(t)\| \leq \beta \ \forall t$. This, in addition to the uniform exponential stability of the unforced system, is sufficient for BIBO stability of our system (Rugh 1996).

The constructive stability condition of (24) is sufficient for system stability (assuming the stability of the individual LTI controllers), but will be conservative. The stability condition assumes that the worst-case switching conditions consistently occur. In practice, we find that the matrix $\hat{M}_{xm}(\Theta_m)$ can be updated continuously with stable performance (as discussed in Section 4). A potential topic for future work is a stability proof that does not rely on the slowly updated $\hat{M}_{xm}(\Theta_m)$ in the proxy controller. Another interesting topic for future work is to show that the system passively interacts with arbitrary users and environments (allowing for intentional power scaling)—that is, that the system is unconditionally stable. The nonlinear nature of the controller makes this a challenging problem. This topic is discussed further in Section 2.4.

2.3. Control Algorithm for Admittance-type Slave

When the slave manipulator is an admittance-type robot, we assume that it is nonbackdrivable (that is, it is not affected directly by external loads) and that the velocity of the end-effector is controlled by a high-bandwidth low-level servo controller. Because we have direct control of the slave dynamics, we will not implement a linearizing and decoupling controller here. With an impedance-type master, we command the force to the master end-effector directly ($F_{am} = F_{cm}$) as

$$F_{cm} = k_{pm}(X_s/\gamma_v - X_m) - k_{dm}\dot{X}_m + \gamma_f F_e \tag{29}$$

where gains are defined as before. The proxy moves with the programmed dynamics as in (8), where F_{PDm} is now defined as:

$$F_{PDm} = k_{pm}(X_m - X_s/\gamma_v) + k_{dm}\dot{X}_m. \tag{30}$$

Figure 5 shows a block diagram of Pseudo-admittance control with an admittance-type slave. The individual controllers are:

$$c_{ms}(s) = \frac{k_{pm}}{\gamma_v s} \tag{31}$$

$$c_{mm}(s) = \frac{k_{dm}s + k_{pm}}{s} \tag{32}$$

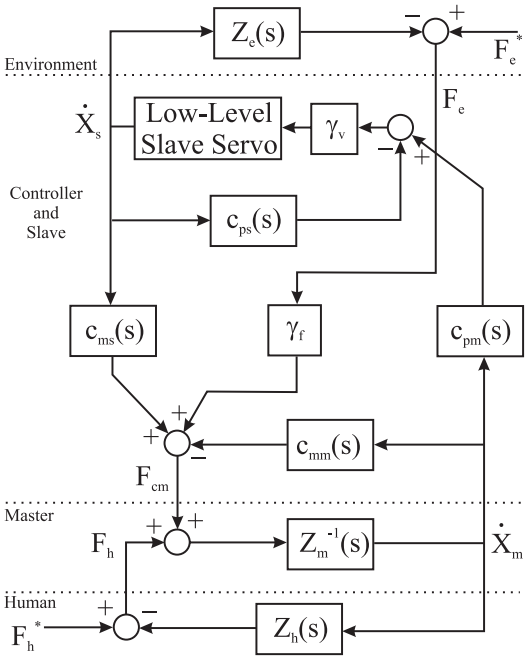

Fig. 5. Block diagram of Pseudo-admittance bilateral telemanipulation with an admittance-type slave.

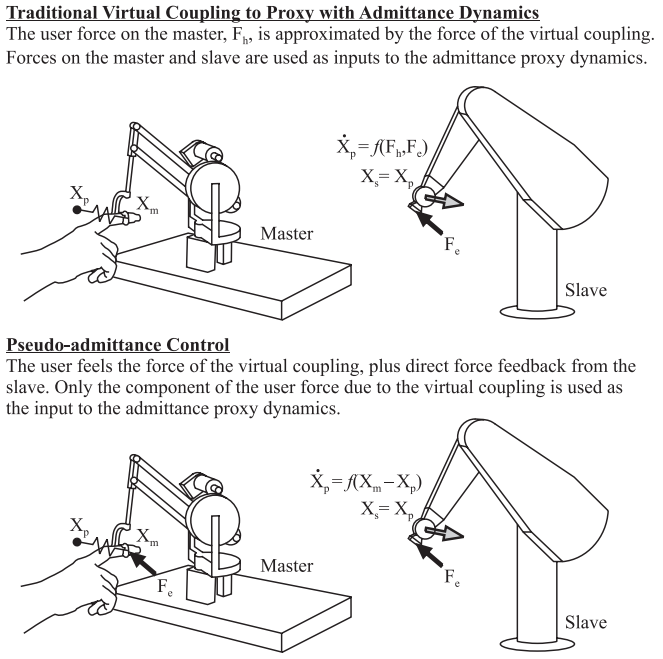

Fig. 6. Pseudo-admittance control with an admittance-type slave compared to traditional schemes using a virtual coupling to a proxy with admittance dynamics. Since the slave position corresponds to the proxy position, the master-coupled-to-slave controller reduces to a master-coupled-to-proxy controller. The master and slave are not drawn to scale.

$$c_{pm}(s) = \alpha\left(\frac{k_{dm}s + k_{pm}}{s}\right) \tag{33}$$

$$c_{ps}(s) = \frac{\alpha k_{pm}}{\gamma_v s}. \tag{34}$$

Note that, while the portion of Figure 5 labeled "Controller and Slave" is LTI, the human and environment impedances Z_h and Z_e are time-varying in general, and the master device impedance Z_m varies across the workspace in general. We will exploit the LTI nature of the "Controller and Slave" in the next section.

Figure 6 compares Pseudo-admittance with an admittance-type slave to an implementation of (1) and (2) using a virtual coupling to a proxy. Because the slave position corresponds to the proxy position, coupling the master to the slave reduces to coupling the master to the proxy. This makes Pseudo-admittance with an admittance-type slave more similar to standard proxy/virtual-coupling schemes than is found with an impedance-type slave.

2.4. Stability for Admittance-type Slave

The simplifying assumptions used with an admittance-type slave allow a simpler stability analysis than with an impedance-type slave. In fact, we can demonstrate robust stability using unconditional stability. Unconditional stability of a telemanipulator implies stable interaction with any passive

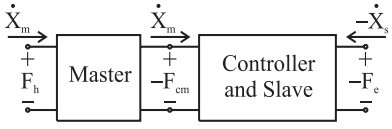

Fig. 7. Two-port-network representation of a telemanipulator with an impedance-type master and an admittance-type slave.

user and environment (Hashtrudi-Zaad and Salcudean 2001). The unconditional-stability criteria provide a powerful stability analysis tool for telemanipulation systems with any master/slave device causality, but the two-port network must be accurately modeled as LTI. Consider the telemanipulator of Figure 5, which is shown in its two-port-network representation in Figure 7. Due to the passivity of the master haptic device, it is sufficient to demonstrate unconditional stability of the "Controller and Slave" two-port of Figure 7, if the goal is to demonstrate unconditional stability of the telemanipulator. However, this may be conservative since the haptic device contains the ability to dissipate energy through friction.

Since the "Controller and Slave" can be decoupled along individual axes (the nonlinearities of the slave manipulator are hidden by the low-level slave servo controller), we may an-

alyze the system using scalar formulas. We can express the "Controller and Slave" two-port using a hybrid matrix:

$$\begin{bmatrix} -F_{cm} \\ -V_s \end{bmatrix} = \begin{bmatrix} h_{11} & h_{12} \\ h_{21} & h_{22} \end{bmatrix} \begin{bmatrix} V_m \\ -F_e \end{bmatrix} \tag{35}$$

with the hybrid matrix parameters

$$h_{11} = \frac{k_{dm}s + k_{pm}}{s + \alpha k_{pm}} \tag{36}$$

$$h_{12} = \gamma_f \tag{37}$$

$$h_{21} = -\gamma_v \alpha \left(\frac{k_{dm}s + k_{pm}}{s + \alpha k_{pm}} \right) \tag{38}$$

$$h_{22} = 0. \tag{39}$$

The two-port network is unconditionally stable if and only if

- the parameters h_{11} and h_{22} have no poles in the open right half plane,
- any poles of h_{11} and h_{22} on the imaginary axis are simple with real and positive residues, and
- the inequalities

$$\mathbb{R}\{h_{11}\} \geq 0 \tag{40}$$

$$\mathbb{R}\{h_{22}\} \geq 0 \tag{41}$$

$$2\mathbb{R}\{h_{11}\}\mathbb{R}\{h_{22}\} - \mathbb{R}\{h_{12}h_{21}\} - |h_{12}h_{21}| \geq 0 \tag{42}$$

hold on the $j\omega$ axis for all $\omega \geq 0$.

We see by inspection that each of the criteria but (42) is satisfied under the assumption of positive gains. After some manipulation, we find that we must also assert that $k_{dm} = 1/\alpha$ to satisfy (42).

The unconditional stability of the telemanipulator demonstrated above requires an accurate LTI model of the system. We must ensure that the proxy velocity always stays within the range that is achievable by the low-level slave servo controller. In addition, the assumption that F_e does not directly affect the slave manipulator assumes an environment that is sufficiently compliant compared to the slave.

2.5. Pseudo-admittance System Characteristics

In this section we explore analytically some of the distinguishing characteristics of this telemanipulation scheme—namely quasi-static transparency, mimicking of admittance control, and steady-hand behavior. Recall that "pseudo-admittance" refers to the mimicking of the admittance control of (1)–(2), "quasi-static transparency" refers to the position and force correspondence between the master and slave at static equilibria, which is closely approximated at slow velocities, and "steady-hand" behavior refers to the attenuation of user hand tremor at the slave. These properties are shown through experiment and simulation in Section 4.

2.5.1. Impedance-type Slave

We begin by considering the static equilibrium points for our system. If we assume a perfect implementation of the master's Cartesian inertia matrix ($\hat{M}_{xm} = M_{xm}$) in the proxy dynamics, a static equilibrium is defined by $[\dot{E}^T \ \dot{X}_p^T]^T = 0$. Assuming α is positive, static equilibrium only occurs when $F_h = -\gamma_f F_e$, and the associated static equilibrium state vector is

$$\begin{bmatrix} \dot{E}_m \\ E_m \\ \dot{X}_s \\ E_s \\ X_p \end{bmatrix} = \begin{bmatrix} 0 \\ 0 \\ 0 \\ M_{xs}^{-1} F_e / k_{ps} \\ (X_s - M_{xs}^{-1} F_e / k_{ps})/\gamma_v \end{bmatrix}. \tag{43}$$

Thus, there is a unique static equilibrium associated with each slave position. At this static equilibrium, the proxy is at a position such that the human exactly feels the scaled slave/environment force ($F_h = -\gamma_f F_e$) and there is perfect position correspondence between the master and the slave ($E_m = 0$) in their respective workspaces. These two properties define the first component of quasi-static transparency. The existence of these static equilibria assumes that the robots are capable of applying the desired forces. If the actuators saturate, the system loses control authority to drive $E_m \to 0$; in this case, the proxy position could grow unbounded as well.

To show that this system mimics admittance control, let us consider the system that has converged on a constant velocity. For a given constant input vector, the equilibrium state, such that $\dot{E} = 0$, is found to be

$$\begin{bmatrix} \dot{E}_m \\ E_m \\ \dot{X}_s \\ E_s \end{bmatrix} = \begin{bmatrix} 0 \\ -M_{xm}^{-1}(F_h + \gamma_f F_e)/k_{pm} \\ \gamma_v \alpha (F_h + \gamma_f F_e) \\ (M_{xs}^{-1} F_e - \gamma_v k_{ds} \alpha (F_h + \gamma_f F_e))/k_{ps} \end{bmatrix}. \tag{44}$$

For a given set of input forces, (44) represents the local equilibrium state associated with a given master and slave position. However, this state will only perfectly satisfy $\dot{E} = 0$ when $\dot{M}_{xm} = 0$ and $\dot{M}_{xs} = 0$. If the system moves slowly across the workspace (or if the Cartesian inertia matrices are constant),

the equilibrium velocity is closely approximated. The values of E_m and E_s vary across the workspace for the same input forces, due to the effects of the underlying linearizing and decoupling controller. The velocity of the slave tends to move under the admittance-control paradigm of (2) as we move slowly across the workspace, giving the desired system performance. $\dot{E}_m = 0$ is equivalent to $\gamma_v \dot{X}_m = \dot{X}_s$, so the master tends to move under the admittance-control paradigm of (1) as well, as we move slowly across the workspace.

We found above that $E_m = 0$ at static equilibrium. This is not the case when the system is moving. In fact, the position error E_m is used to drive the movement of the system (see (8, 9)). The position error E_m is related to the applied forces, and consequently, the velocity of the system. As we apply small forces (that is, when the difference between F_h and $-\gamma_f F_e$ is small), E_m becomes small, and the system moves slowly across the workspace. This in turn leads to the steady-state velocity properties discussed above. This is the second component of quasi-static transparency: as the velocity of the system is reduced, the system approaches perfect transparency.

It is reasonable to wonder if a switch between controllers, due to the slow update rate of $\hat{M}_{xm}$ in the proxy dynamics, will create an impulse that will add noise to the system that is possibly felt by the user. An update in $\hat{M}_{xm}$ causes a discontinuity in the proxy velocity of (16), but it does not cause a discontinuity in the proxy position X_p. The slave controller of (5) does not rely on $\dot{X}_p$, so the slave's actuator does not display a discontinuity. The master servos to the slave, so it does not experience a discontinuity either. Thus, the user does not feel the switching event.

The integrating nature of the proxy dynamics tends to attenuate and average high-bandwidth movements of the master relative to the slave. In addition, reducing the admittance gain will result in reduced system velocity. These factors create a "steady-hand" behavior in the system. By including direct force feedback, we have provided a means for high-bandwidth haptic information to be relayed to the user.

2.5.2. Admittance-type Slave

Each of the characteristic properties of Psuedo-admittance are retained with an admittance-type slave. Because the slave and proxy positions coincide (with possible scaling) with an admittance-type slave, the analysis required to demonstrate these properties is simpler. We begin by considering the static equilibrium points of our system. We find that the system is only at static equilibrium if $E_m = 0$ and $F_{cm} = \gamma_f F_e$. With an impedance-type master device, we can assume that $F_h \approx -F_{cm}$. Thus, at static equilibrium there is no position error between the master and slave, and the user feels the correct reflected environmental force.

To demonstrate that the system mimics admittance control, let us consider the system that has converged on a constant velocity. In this state, the proxy velocity can be expressed as

$$\dot{X}_p = \alpha(-F_{cm} + \gamma_f F_e). \tag{45}$$

Again, under the assumption that $F_h \approx -F_{cm}$, we find the proxy velocity, and consequently the slave velocity, move with the desired behavior of (2). In this state, E_m is constant for a given set of applied forces, and the master moves with the velocity of (1).

3. Guidance Virtual Fixtures

The Pseudo-admittance controller enables implementation of so-called passive GVFs, which were introduced in Section 1.2. One of the benefits of these admittance-type GVFs is that they do not typically exhibit instabilities like those associated with impedance-type virtual fixtures (Abbott and Okamura 2006). In this section, we extend the GVFs introduced in Bettini et al. (2004), originally designed for admittance-type human-machine cooperative systems, to Pseudo-admittance bilateral telemanipulation. The construction of the the Pseudo-admittance controller, specifically the use of a proxy, lends itself to this type of GVF.

Prior GVF schemes for telemanipulation have put the GVF on either the master or slave side. Our method is different in that the entire system is integrated into the implementation of the GVF. The philosophy behind previous proxy-based GVF methods has been to restrict the proxy to desired subsets of the workspace (described as "virtual fixtures," "virtual mechanisms," etc.) (Micaelli et al. 1998; Turro et al. 2001). However, it may not be desirable to restrict the proxy to the desired path or surface, if our actual goal is to move the slave along the desired path or surface. If the slave robot experiences a disturbance load, that method could actually keep the slave off of the desired path or surface, unless the slave tracks the proxy perfectly. In our method, the proxy has the potential to move anywhere in the workspace, in an attempt to keep the slave moving on the desired path or surface. Allowing the proxy to move anywhere in the workspace also lends itself to GVFs that act as guidance in the truest sense of the word. Our GVF allows the user to maintain ultimate control of the system, since the slave is allowed to potentially move anywhere in the workspace. Our GVF uses instantaneous preferred directions of motion to haptically assist the user in easily moving the slave along desired paths or surfaces, while imposing guarded motion when the user intentionally moves away from the desired path or surface. In general, the desired path or surface that we would like the slave to move along may have any continuous geometry. For brevity, the remainder of this section will refer to the desired path or surface simply as the path. The path can be obtained *a priori* or from sensing during task execution (Bettini et al. 2004); identification of the path is beyond the scope of this work.

Table 2. Definition of variables used in the guidance virtual fixtures. The desired path or surface is described simply as the path.

Variable	Definition
X_s	Position of the slave
X_{vf}	Point on the path closest to the slave
E_{vf}	Error vector pointing from X_s to X_{vf}
F_{PDm}	Component of F_h due to master servo, considered as the input for the GVF
Δ_{vf}	Matrix with columns that form a basis for the instantaneous linear subspace created by the path at X_{vf}
F_Δ	Projection of the input force F_{PDm} into the path space
$\hat{T}_{vf}$	Instantaneous unit-tangent vector to the path
$\hat{P}_{vf}$	Preferred direction of movement (unit vector)
k_{vf}	GVF stiffness, which determines how much the preferred direction of movement points toward the path
F_P	Component of input force F_{PDm} in the preferred direction
$F_{\bar{P}}$	Component of input force F_{PDm} not in the preferred direction
γ_{vf}	Gain attenuating the the force in non-preferred directions
F_{vf}	Force used to command proxy movement
α	Admittance gain

3.1. Implementation

We assume that we can instantaneously find the point on the path that is closest to the slave; we call this point X_{vf} (descriptions of the variable used in the GVFs can be found in Table 2). Finding this closest point constitutes its own field of research in computational geometry (Smid 2000), and we will not address it here. We then define the GVF error as the vector between the slave and the path:

$$E_{vf} = X_{vf} - X_s. \tag{46}$$

The path may be instantaneously defined by a linear subspace described by a $3 \times n$ matrix Δ_{vf}, where the n linearly independent columns form an orthonormal basis for the path space at X_{vf} ($n = 1$ for a line, $n = 2$ for a plane). If the path is not continuously differentiable, additional system intelligence will be required to define Δ_{vf} at any corners.

We will consider the force that the user applies to overcome the master's PD controller, F_{PDm}, as the input to the GVF. If the user is perfectly balancing any reflected environmental force, we have $F_{PDm} = 0$, which is interpreted as no input to the GVF (i.e., no velocity command). We find the projection of the input force into the path space:

$$F_\Delta = \Delta_{vf} \Delta_{vf}^T F_{PDm}. \tag{47}$$

We then construct the instantaneous unit tangent vector to the path as:

$$\hat{T}_{vf} = \begin{cases} \frac{F_\Delta}{\|F_\Delta\|} & : \ \|F_\Delta\| > 0 \\ 0 & : \ \|F_\Delta\| = 0 \end{cases}. \tag{48}$$

We now define the preferred direction of the GVF as

$$P_{vf} = k_{vf} E_{vf} + \hat{T}_{vf} \tag{49}$$

where k_{vf} is the user-defined GVF stiffness. Though this term does not have traditional stiffness units, it does determine how much the preferred direction tries to influence movement back toward the path, as a function of the GVF error E_{vf}. We will make use of the normalized preferred direction:

$$\hat{P}_{vf} = \begin{cases} \frac{P_{vf}}{\|P_{vf}\|} & : \ \|P_{vf}\| > 0 \\ 0 & : \ \|P_{vf}\| = 0 \end{cases}. \tag{50}$$

We next break the input force F_{PDm} into components in the preferred direction

$$F_P = \begin{cases} (\hat{P}_{vf}^T F_{PDm}) \hat{P}_{vf} & : \ \hat{P}_{vf}^T F_{PDm} > 0 \\ 0 & : \ \hat{P}_{vf}^T F_{PDm} \leq 0 \end{cases} \tag{51}$$

and in the nonpreferred directions

$$F_{\bar{P}} = F_{PDm} - F_P. \tag{52}$$

We then construct the GVF force by combining the force in the preferred direction with an attenuation of the force in the nonpreferred directions:

$$F_{vf} = F_P + \gamma_{vf} F_{\bar{P}} \tag{53}$$

where $\gamma_{vf} \in [0, 1]$ is the user-defined GVF attenuation gain. To implement the GVF, we modify the proxy dynamics of (8) to

$$\dot{X}_p = \alpha F_{vf}. \tag{54}$$

Figure 8 provides a geometric depiction of the GVF. If there is a component of the applied force F_{PDm} in the preferred direction, the algorithm maps the applied force into the GVF force F_{vf}, which points more in the direction of the path than did the original. This moves the proxy in a direction that will tend to move the slave (which is servoing to the proxy) towards the path. The applied force is slightly attenuated in magnitude in creating F_{vf}. If there is no component of the applied force F_{PDm} in the preferred direction, the GVF does not change the

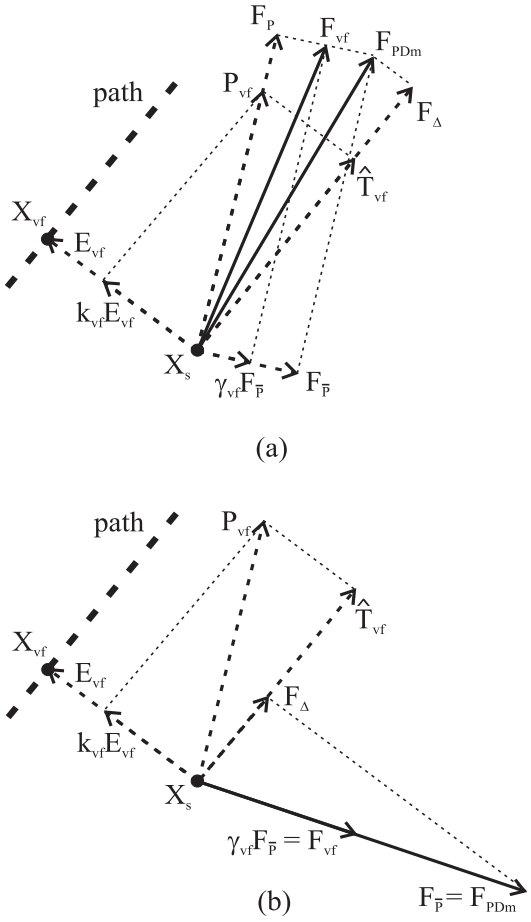

Fig. 8. A geometrical view of guidance virtual fixtures when there (a) is and (b) is not a component of the applied force in the preferred direction. The virtual fixture maps the input force F_{PDm} into the virtual fixture force F_{vf}, which is then used as a command to the proxy.

direction of the applied force, but the magnitude is attenuated by γ_{vf}. Thus, if the user commands a force that is intentionally moving away from the path, the GVF does not guide the user towards the path, but rather, it encourages the user to move in a guarded fashion.

In Section 2.2, we determined that for guaranteed stability with an impedance-type slave, we could restrict the $A(t)$ matrix to be LTI for sufficient durations of time. This was accomplished by updating time-varying elements in the proxy dynamics at a slower rate. Though the implementation is slightly different, the GVFs introduced in this section are simply a state-dependent adaptation of the proxy dynamics. For the guaranteed stability result of Section 2.2, we must ensure that $A(t)$ is still LTI for sufficient durations of time. To accomplish this, the $\hat{M}_{xm}$ matrix should still be updated with period τ, and

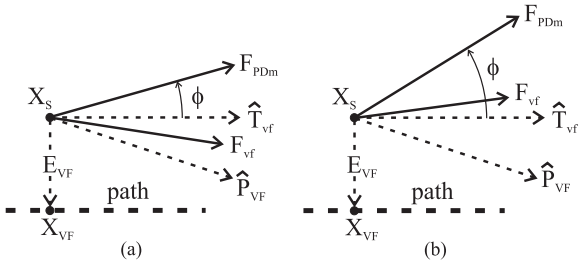

Fig. 9. The user applies a unit-magnitude force F_{PDm}, and the GVF maps the applied force into the proxy command force F_{vf}. (a) If the angle ϕ is sufficiently small, the GVF tends to be attractive. (b) If the angle ϕ is too large, the proxy is commanded away from the path.

in addition, the preferred direction of the GVF (49) should also be updated with a period τ, with an impendance-type slave.

3.2. Attractivity

The purpose of the GVF is to guide the user along a desired path, yet we have designed a GVF method that allows the user to potentially move the slave anywhere in the workspace. It is reasonable to wonder how well our GVF works in serving its intended purpose. In this section, this concern is addressed and quantified. If, with some initial error E_{vf}, the user attempts to command the slave along the path, we would hope that the slave converges to the path, or at the least, moves parallel to it; it would be undesirable if the slave actually diverged from the path. But human force-direction perception is imprecise (Tan et al. 2006), and the actual commanded force F_h could be in a different direction than the intended commanded force/velocity. In this section we quantify the robustness of GVF attractivity to errors in the direction of the commanded force.

Consider Figure 9, where the user applies a unit-magnitude force that is ϕ radians away from parallel to the desired path. For simplicity, we only consider the 2-D case, but the extension to higher dimensions (i.e., when the GVF is on a surface) is clear. In this section, we explicitly consider a linear path, under the assumption that the path is smooth and locally linear. We would like to quantify for what angles ϕ the resulting F_{vf} would actually tend to increase $\|E_{vf}\|$ by commanding the proxy away from the path. For this section, we use the notation $s\phi = \sin\phi$, $c\phi = \cos\phi$, $t\phi = \tan\phi$.

We are particularly interested in the sign of the vertical component of the force F_{vf} resulting from the force F_{PDm} in Figure 9. If this vertical component is negative, the proxy will be commanded to move towards the path; if the vertical component is positive, the proxy will be commanded to move away from the path. We begin by writing (53) as

$$F_{vf} = (1 - \gamma_{vf})(\hat{P}_{vf}^T F_{PDm})\hat{P}_{vf} + \gamma_{vf} F_{PDm} \qquad (55)$$

where the unit-magnitude F_{PDm} can be written as

$$F_{PDm} = [c\phi \quad s\phi]^T \tag{56}$$

and (49) can be rewritten in vector form:

$$P_{vf} = \begin{bmatrix} 1 & -k_{vf}e_{vf} \end{bmatrix}^T \tag{57}$$

where $e_{vf} = \|E_{vf}\|$. After some manipulation, we create an intermediate vector

$$\begin{aligned} F'_{vf} &= (1-\gamma_{vf})(c\phi - k_{vf}e_{vf}s\phi)\begin{bmatrix} 1 \\ -k_{vf}e_{vf} \end{bmatrix} \\ &+ \gamma_{vf}(1+k_{vf}^2e_{vf}^2)\begin{bmatrix} c\phi \\ s\phi \end{bmatrix} \end{aligned} \tag{58}$$

where

$$F'_{vf} = \|P_{vf}\|^2 F_{vf} \tag{59}$$

is simply a positively scaled version of F_{vf}. Since the sign of the vertical component of F_{vf} indicates whether it points toward or away from the path, we consider the vertical component of F'_{vf}:

$$f'_{vf} = k_{vf}^2e_{vf}^2s\phi + (\gamma_{vf}-1)k_{vf}e_{vf}c\phi + \gamma_{vf}s\phi. \tag{60}$$

We note that if $\phi = 0$, then

$$f'_{vf} = (\gamma_{vf}-1)k_{vf}e_{vf} \tag{61}$$

is always negative. In other words, the GVF is always attractive if the commanded force does not point away from the path, which comes as little surprise. We also note that, if $e_{vf} = 0$, then

$$f'_{vf} = \gamma_{vf}s\phi \tag{62}$$

is always positive if $\phi > 0$ and $\gamma_{vf} \neq 0$. In other words, the slave can always be commanded to leave the path if $\gamma_{vf} \neq 0$. In general, if $\phi > 0$, then $c\phi > 0$ and we can divide (60) by $c\phi$ to get a positively scaled version of f'_{vf}:

$$f''_{vf} = k_{vf}^2t\phi e_{vf}^2 + (\gamma_{vf}-1)k_{vf}e_{vf} + \gamma_{vf}t\phi. \tag{63}$$

This is a quadratic function in e_{vf}, and because of the positive scalings in the preceding derivation, the sign of f''_{vf} is the same as the sign of the vertical component of F_{vf}.

Figure 10 shows a visualization of the quadratic function (63). The roots of (63) are found as

$$e_{1,2} = \frac{1-\gamma_{vf}}{2k_{vf}t\phi} \pm \frac{((1-\gamma_{vf})^2 - 4\gamma_{vf}t^2\phi)^{\frac{1}{2}}}{2k_{vf}t\phi} \tag{64}$$

where the "+" corresponds to e_{crit}, and the "−" corresponds to e_{conv}, in Figure 10(a). If

$$(1-\gamma_{vf})^2 - 4\gamma_{vf}t^2\phi < 0 \tag{65}$$

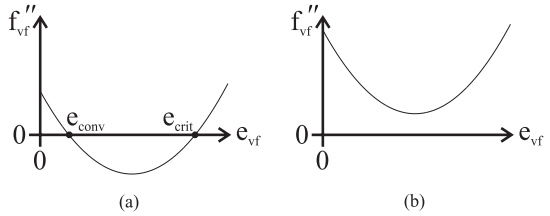

Fig. 10. Visualization of the quadratic function (63), when (a) $(1-\gamma_{vf})^2 - 4\gamma_{vf}t^2\phi \geq 0$, and when (b) $(1-\gamma_{vf})^2 - 4\gamma_{vf}t^2\phi < 0$. A positive f''_{vf} tends to increase e_{vf}.

then the roots of (64) are imaginary, and we have curve of Figure 10(b), indicating that e_{vf} will continue to grow (i.e., the proxy diverges from the path). This condition can be rewritten as a condition on ϕ for a given γ_{vf}:

$$\phi > \text{atan}\left(\frac{1-\gamma_{vf}}{2}\left(\frac{1}{\gamma_{vf}}\right)^{\frac{1}{2}}\right). \tag{66}$$

Thus, for each value of γ_{vf} there exists some ϕ above which the proxy will diverge from the path (regardless of the value of k_{vf} or e_{vf}). When the roots of (64) are real, we have curve of Figure 10(a). For a given set of k_{vf}, γ_{vf}, and ϕ, if the proxy error is greater than the critical value ($e_{vf} > e_{\text{crit}}$) then the proxy will diverge from the path, and if the proxy error is less than the critical value ($0 \leq e_{vf} < e_{\text{crit}}$) then e_{vf} will converge on e_{conv}.

From the preceding analysis, we find that given a set of k_{vf} and γ_{vf}, as well as a bound on the possible values that ϕ might take, we can find a bounded region of magnitude e_{conv} such that if we begin within this region, then we are ensured to stay within this region. In addition, whenever the value of ϕ decreases, the magnitude of the error bound also decreases.

4. Experimental Verification

In this section we verify the properties of Pseudo-admittance control, with and without GVFs, through both simulations and experiments.

4.1. Experimental Setup

The experimental system that we consider is constructed of two PHANToM robots from SensAble Technologies, shown in Figure 11. The master device is a PHANToM Premium 1.0, and the slave device is a PHANToM Premium 1.5. These robots have identical kinematics, but the workspace of the PHANToM 1.5 is 50% larger than that of the PHANToM 1.0, and the other robot parameters are scaled accordingly. The PHANToMs are run on a single computer, at a sampling rate

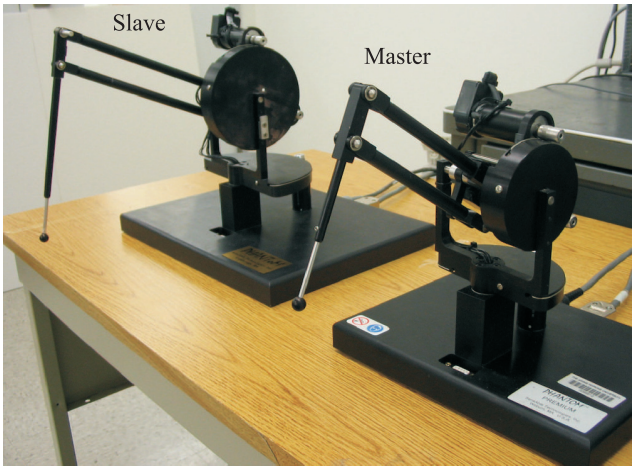

Fig. 11. Experimental setup consisting of two PHANToM robots.

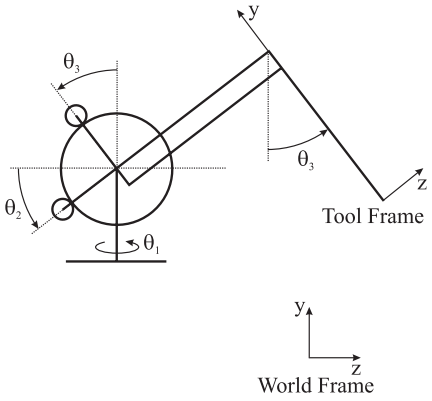

Fig. 12. PHANToM frame description, assuming right-handed coordinate systems. The tool frame coincides with the world frame at the zero position of the PHANToM.

of 500 Hz. In addition to the experimental system, we have constructed a MATLAB simulation of our system. This allows us to explore certain aspects of system performance in a more controlled setting. All experiments and simulations use $\gamma_v = 1$. Figure 12 shows the PHANToM coordinate system frames used throughout. By synthesizing two prior works (Craig et al. 1987; Cavusoglu et al. 2002), we implemented an adaptive algorithm, run off-line, to obtain the necessary PHANToM parameters for the control system and the simulation; details can be found in (Abbott 2005).

For our system, the servo gains for the linearizing and decoupling controller were chosen empirically. The values chosen are $k_{dm} = k_{ds} = 150\,\text{N·s/(m·kg)}$ and $k_{pm} = k_{ps} = 5625\,\text{N/(m·kg)}$; these are not typical servo gain units, but rather, they are the servo gains that act on the linear and decoupled unit-mass system. These gains were chosen such that the individual systems are critically damped (assuming a stationary proxy), and they were chosen to be as high as possible before sampling and quantization effects start to noticeably degrade the system's behavior. These gains are used throughout the experiments and simulations to follow.

After choosing the PD servo gains, the next step is to find the fastest rate at which we may update our proxy dynamics and still guarantee stability of the nonlinear, time-varying system. To quantify the bounds of (24), we numerically evaluated the norm of the matrix $A(t)$ at hundreds of locations across the workspace of the master device as described in Section 2.2, with the largest values of α to be used in this section, and it was determined that an update rate of 10 Hz ($\tau = 0.1$ seconds) of the parameter $\hat{M}_{xm}(\Theta_m)$ in the proxy dynamics will result in a guaranteed stable system. This value was used in the experiments and the simulations to follow. We found that the location in the robot workspace actually had little effect on the value of τ needed to satisfy (24); the norm of $A(t)$ was dominated by the servo gains. Also, in practice we find that we can update $\hat{M}_{xm}(\Theta_m)$ in the proxy dynamics continuously (that is, at every sample) with no perceived degradation in stability. The condition of (24) is simply a sufficient condition; a nonlinear stability proof that does not rely on (24) is left as a topic for future consideration.

To obtain our measurement of the environmental force F_e in our experimental setup, we use the force generated at the tool tip by the slave's actuators as an approximation of the true force. For our slow-moving, low-inertia, low-friction PHANToMs, this is a good approximation for the purposes of this controller.

4.2. Pseudo-admittance Bilateral Telemanipulation

We begin by demonstrating the steady-hand properties of Pseudo-admittance. Figure 13 shows the master and proxy positions in the three coordinate axes as the user moves the telemanipulator across the workspace. The slave is moving in free space, and it closely follows the proxy. The user displays hand tremor that is greatly attenuated in the proxy. Also, at approximately the 5 s mark, the user releases the master, and the system stays in place, confirming the stability of the system.

Ideally the proxy velocity is, by definition, proportional to the applied force F_{PDm} through (8). But to guarantee stability, we choose to update the proxy dynamics at a slower rate. Figure 14 shows that this does not significantly impact on the performance of the system. In the figure, we see the proxy velocity along the three coordinated axes, plotted against the applied force F_{PDm} normalized by the admittance gain α. If the proxy dynamics were updated continuously, these two values would perfectly coincide. In this figure we see that the proxy velocity shows very little differences with the commanded velocity. In fact, every 0.1 seconds (that is, at every update of the proxy dynamics), the two variables coincide.

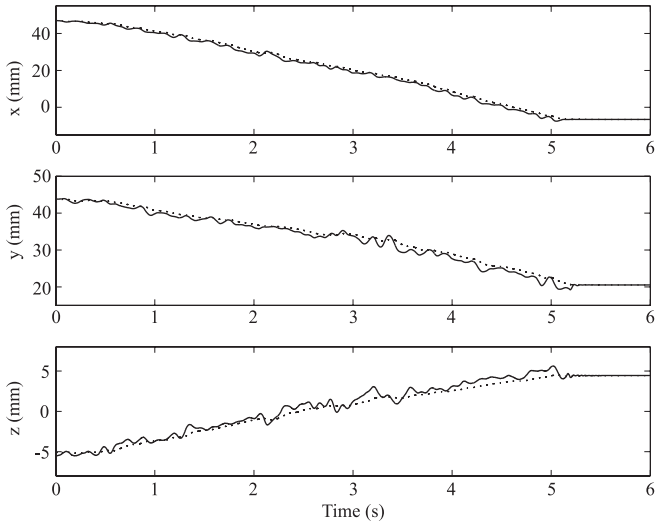

Fig. 13. An experimental demonstration of the steady-hand behavior seen in Pseudo-admittance control ($\alpha = 30\,\text{mm/(N·s)}$). Master (—) and proxy ($\cdots$) trajectories are shown as the user attempts to command the system to move at a constant velocity across the workspace between two arbitrary points. The proxy behavior is significantly steadier than the master.

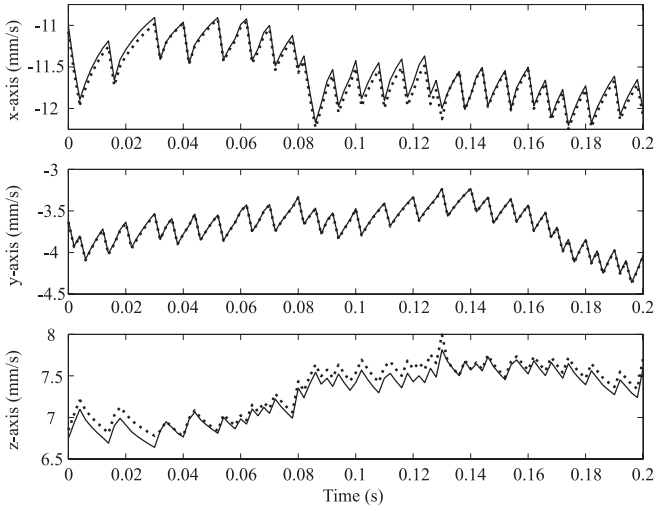

Fig. 14. Effects of slow update rate in proxy dynamics ($\alpha = 30\,\text{mm/(N·s)}$). Normalized force F_{PDm}/α (—) and proxy velocity ($\cdots$) show little difference. Data is taken from the data set of Figure 13.

The human user is an integral component in this human–machine collaborative system, but human motions and physical parameters are also highly variable. We have created a simulation for our PHANToM telemanipulation system that allows us to obtain less anecdotal results than we would obtain from experiments alone. We make use of our simulation now to consider, in a controlled fashion, the behaviors of the Pseudo-admittance bilateral telemanipulation system when interacting with various types of environments.

Figure 15 shows how our system interacts with purely viscous environments. We include damping $b_e = 0\,\text{Ns/m}$, which is the slave moving freely in space. For each simulation, the PHANToMs begin in the zero position, embedded in the simulated environment. The user applies a constant force F_h in the x direction of the world frame for the first three seconds, and then releases the device ($F_h = 0$). The plot shows the position in the x direction of the world frame. From these plots, the nature of the Pseudo-admittance controller becomes clear. The slave moves with a velocity that is almost perfectly linearly proportional to the applied forces. The position error between the master and slave is used to drive that movement. When the master is released, the position error disappears, and the system stays where it was released by the user.

As the value of the admittance gain α is increased, the system moves faster, and it is easier to distinguish the two different viscosities, since the environmental force is proportional to the speed of the slave. The position error generated between the master and slave by the user's applied force is unchanged, but it appears to be reduced because it is smaller relative to the total distance traveled. Increasing the force feedback gain γ_f has no effect when the slave is moving in free space, but does result in slower velocities when the slave is moving through a viscous environment. Increasing γ_f also has the effect of reducing the position error between the master and the slave while moving. This makes sense, since a larger portion of the applied force F_h is going towards balancing the force $\gamma_f F_e$, leaving less force for generating a position error in the master's servo controller. The effect of pushing harder (increasing F_h) is faster movement, with larger associated position errors between the master and the slave. However, from the plots it is evident that the increase in position error is proportional to the increase in velocity, so that the relative behavior of the system is essentially unchanged by a change in the applied force.

Figure 16 shows how our system interacts with purely elastic environments. We simulate a unilateral spring surface that pushes in the $-x$ direction of the world frame when the slave enters the $+x$ half-space. For each simulation, the PHANToM begins in the zero position, at the surface of the simulated environment. The user applies a constant force F_h in the $+x$ direction of the world frame for the first two seconds, and then releases the device ($F_h = 0$). The plot shows the position in the x direction of the world frame. It is evident that a constant input force F_h does result in a static equilibrium with an elastic environment. In addition, the position error between the master and the slave vanishes. The proxy reaches into the environment, pulling the slave behind it, until the force generated is large enough to drive the master back into static equilibrium. When the master device is released with potential energy stored in the

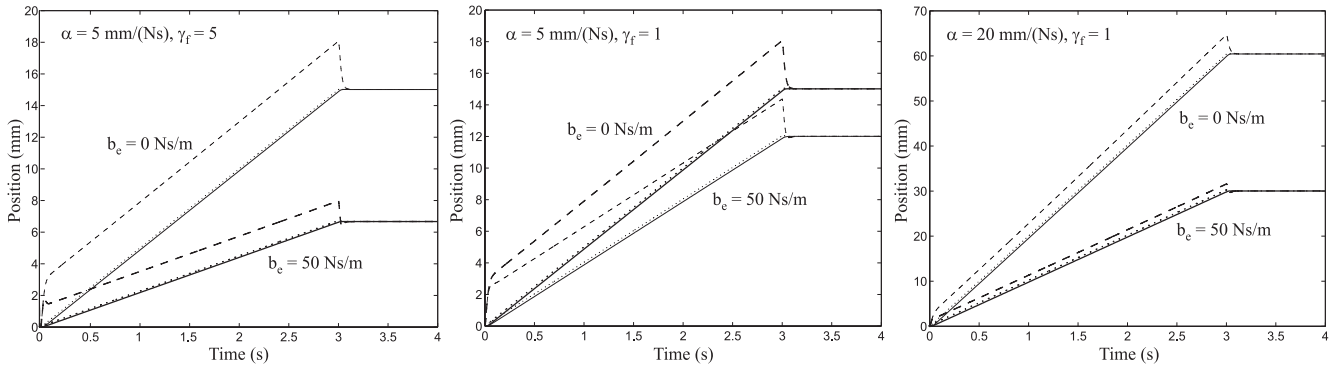

Fig. 15. Simulated interactions with viscous environments with damping b_e. Master (- -), slave (—), and proxy ($\cdots$) trajectories are shown. The user applies a constant force $F_h = 1$ N for the first three seconds, and then releases the master. Note that the scaling differs between plots.

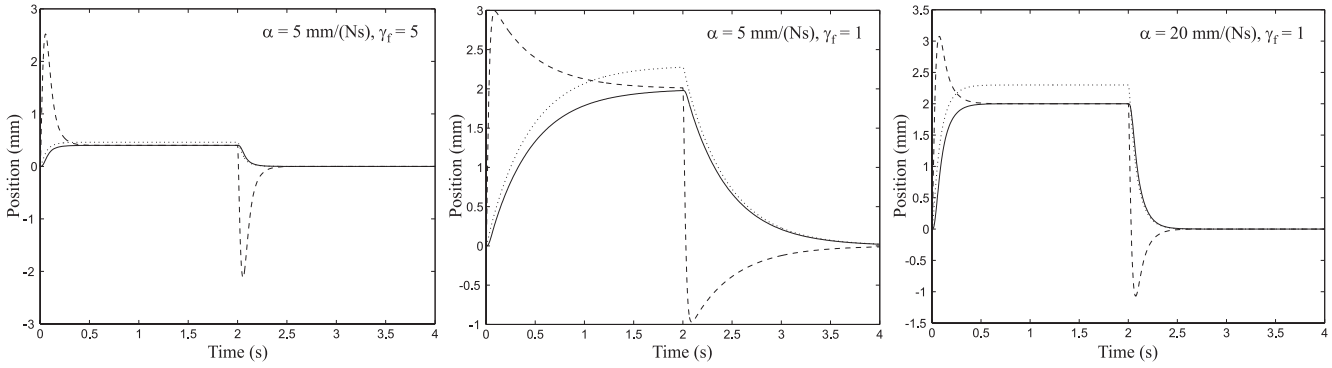

Fig. 16. Simulated interactions with elastic environment with spring constant $k_e = 500$ N/m. Master (- -), slave (—), and proxy ($\cdots$) trajectories are shown. The user applies a constant force $F_h = 1$ N for the first two seconds, and then releases the master. Note that the scaling differs between plots.

environment, the environment pushes the slave out to the surface. The master is temporarily pushed well outside the boundaries of the environment by the force-feedforward term, but the position error between the master and the slave eventually vanishes, with the system coming to rest just outside the elastic environment. In practice, a dead-man switch should be used to only allow proxy movement when the user is holding the master.

It is clear that the static equilibrium position is independent from the admittance gain α; the admittance gain simply governs how quickly static equilibrium is reached. In fact, increasing either α or γ_f decreases the rise time of the system. Changing the magnitude of the input force F_h results in a change in equilibrium position, but the relative time response is unchanged. Changing γ_f also changes the equilibrium point; changing γ_f effectively changes the stiffness of the environment.

Figure 17 shows experimental data of our PHANToM telemanipulation system interacting with a stiff tabletop. Figure 17(a) shows position data for four combinations of admittance gain and commanded velocity. The data shows that the slave movement is steadier than the master. The data also shows the proxy moving down below the surface of the table to a depth proportional to the user's applied force. The experimental system exhibits the same behavior as predicted by the simulations. It is evident that combining low values for α and fast commanded movements leads to the largest discrepancies between master and slave. Figure 17(b) shows force data normal and tangent to the tabletop for one of the data sets in Figure 17(a). We can clearly see the regions where the user is commanding force largely in the normal or tangent directions. In this figure, the applied forces F_h is approximated by $-F_{cm}$. We also see in Figure 17(b) that the user must apply a force away from the surface to move the slave quickly away from the surface. This

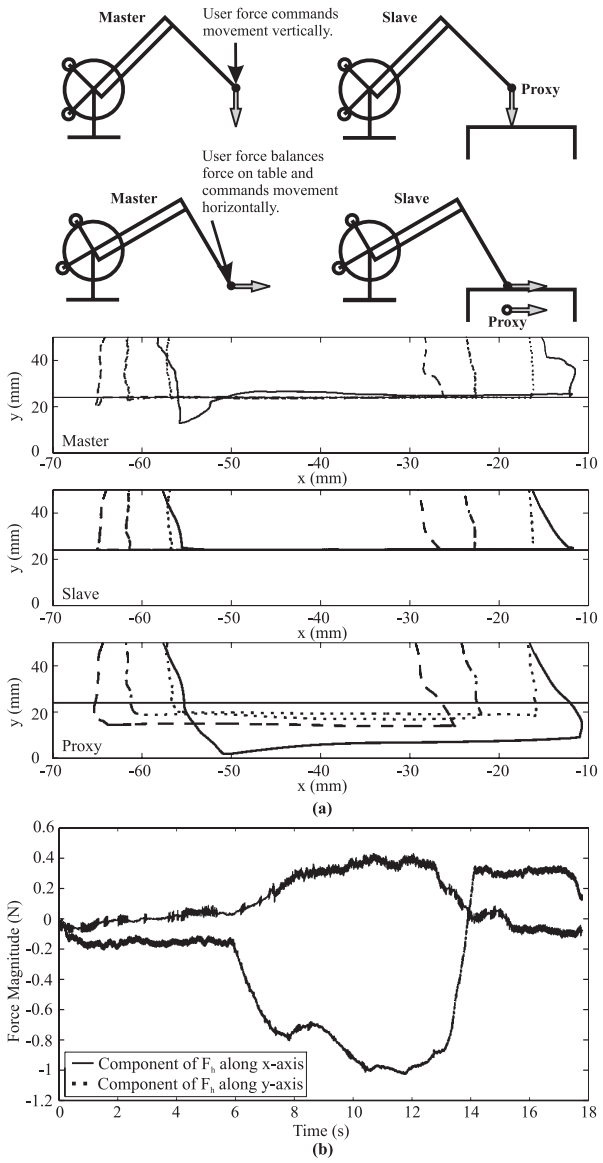

Fig. 17. Experimental data showing interaction with a stiff environment. The user commands the slave down to the tabletop shown in Figure 11, across the table from left to right, and back off of the table. (a) Position data is shown for various α and velocity: (—) shows $\alpha = 40\,\text{mm/(N·s)}$ with a completion time of 7 s, (–·) shows $\alpha = 40\,\text{mm/(N·s)}$ with a completion time of 18 s, (––) shows $\alpha = 120\,\text{mm/(N·s)}$ with a completion time of 4.5 s, and (···) shows $\alpha = 120\,\text{mm/(N·s)}$ with a completion time of 16 s. The tabletop at $y = 24\,\text{mm}$ is also shown. (b) Force data is shown versus time for the data set with $\alpha = 40\,\text{mm/(N·s)}$ with a completion time of 18 s.

is perceived as a stickiness of the surface. If the user attempts to move the slave away slowly, this effect is reduced (as part of the quasi-static transparency of the system). Note that the

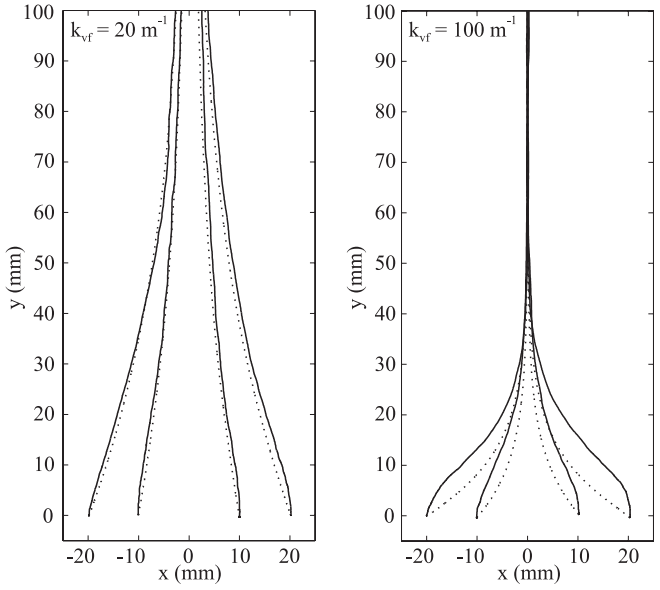

Fig. 18. Experimental data showing GVFs for the vertical plane defined by $x = 0$. Master (—) and proxy (···) trajectories are shown. From each of the initial positions at the bottom of the plots, the user applies a gentle force in approximately the $+y$ direction and is guided to the desired plane by the GVF. Data is shown for $\gamma_{vf} = 0.05$ and $\alpha = 40\,\text{mm/(N·s)}$. The slave is moving freely.

admittance perceived by the user when commanding the slave to move away from the table is higher than α, due to the direct feedback of F_e. This provides the user with haptic information about F_e, without providing traditional transparency.

4.3. Guidance Virtual Fixtures

We begin with the implementation of a basic GVF—a vertical plane—on our experimental system. The desired surface is a vertical plane defined by $x = 0$ in the world frame. We describe the GVF surface by:

$$\Delta_{vf} = \begin{bmatrix} 0 & 0 \\ 1 & 0 \\ 0 & 1 \end{bmatrix}. \tag{67}$$

We implement the GVF on a Pseudo-admittance telemanipulator with admittance gain $\alpha = 40\,\text{mm/(Ns)}$.

Figure 18 shows GVFs implemented with two different k_{vf} values. In each plot, we start at rest (at four different initial conditions) near the bottom of the plot. Then the user simply applies a gentle force in approximately the positive y direction of the world frame. The plots show the resulting movement of

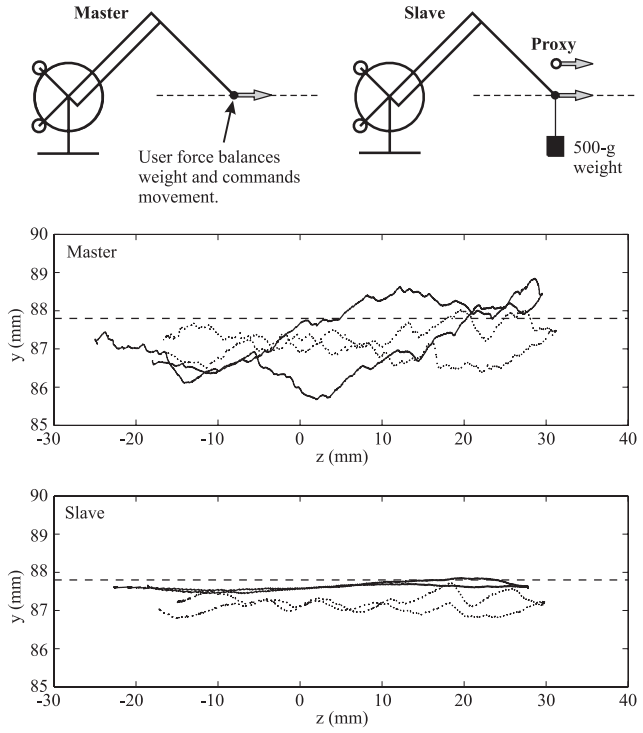

Fig. 19. Experimental data showing the effectiveness of a GVF when the slave experiences a load. The GVF is defined by the plane $y = 87.8$ mm, shown by (– –). A 500 g weight hangs from the tip of the slave manipulator. The user commands the slave to move from left to right (in the figure), and then back from right to left, while attempting to keep the vertical (y) position of the slave constant with direct visual feedback. Data is shown for $\alpha = 40$ mm/(N·s) and $k_{vf} = 0.1\,\mathrm{m}^{-1}$. (—) shows $\gamma_{vf} = 0.05$ with a completion time of 16 s. ($\cdots$) shows $\gamma_{vf} = 1$ (no virtual fixture) with a completion time of 20 s.

the master device, as well as the proxy (to which the slave servos). It is evident from the figure that increasing k_{vf} points the preferred direction more towards the desired plane than parallel to it. Reducing γ_{vf} has a similar but smaller effect by attenuating the component of the input force, and consequently the commanded velocity, in the the non-preferred directions. The benefits of these GVFs are evident; the device closely approaches the desired surface with essentially no cognitive effort on the part of the user. Recall that the user has complete control to move the device away from the plane at all times; these are simply the paths that the robots favor.

From the figure, it appears that increasing k_{vf} tends to increase the position error between the master and the proxy (and consequently between the master and the slave). But recall that the position error is proportional to the applied force, under the quasi-static assumption of the slow-moving proxy. The position error seen in this figure is simply due to the large components of the applied force in the non-preferred direction. The lower values of k_{vf} have similar position errors – they are simply more aligned with the direction of motion.

These novel GVFs are also effective when the slave is experiencing an environmental load. Figure 19 shows the user commanding the slave to move across a horizontal plane defined by the GVF surface

$$\Delta_{vf} = \begin{bmatrix} 1 & 0 \\ 0 & 0 \\ 0 & 1 \end{bmatrix}. \tag{68}$$

The user has direct visual feedback of the slave, but no reference as to where the desired plane is. A 500 g weight hangs from the slave manipulator, pulling the slave away from the desired plane. The user feels all of the weight ($\gamma_f = 1$), and has control to move the slave anywhere in the workspace, but the GVF helps steady the slave and keep it moving near the desired plane.

5. Conclusions

In this paper, we presented a novel bilateral telemanipulation control system called Pseudo-admittance. This system is designed to mimic admittance control on systems where the master is an impedance-type robot. It has many desirable properties, such as steady-hand tremor attenuation, quasi-static transparency, and the ability to include guidance virtual fixtures. A novel guidance virtual fixture method was presented that builds upon a method previously developed for human–machine cooperative systems. The properties of Pseudo-admittance bilateral telemanipulation, with and without guidance virtual fixtures, were verified through simulations and experiments on a system where both the master and slave are of the impedance type. Pseudo-admittance has potential benefits for systems that are designed for stability and transparency, but that require better-than-human levels of precision during the execution of certain tasks. Pseudo-admittance could also be applied to systems with large motion scaling or velocity limits at the slave, systems that are typically run under rate control. Guidance virtual fixtures could be used as task macros, potentially increasing both speed and precision on structured tasks that still require direct human control.

Qualitatively, this system feels very stable; in free space it feels almost like a pure, high viscosity. The system interacts well with any environment (including rigid surfaces) for a large range of admittance gain values. While the control system does not exhibit transparency in the traditional sense, it does provide the user with a rich set of haptic information. As the user pushes the slave into an environment, the user feels a lower perceived admittance than in free space. If the user then moves the slave away from the surface, the user feels an increased admittance due to the direct feedback

of the slave/environment force. In this sense, the information about the force on the environment is presented to the user through changes in perceived admittance. Pseudo-admittance is specifically designed to assist the user with precise, slow-moving tasks, and consequently the system provides the best sense of telepresence for the user when commanded to move at slow velocities.

A remaining question is how best to control orientation of the end effector under Pseudo-admittance control. Because of the non-commuting nature of rotations, it is not clear if Pseudo-admittance translates to orientation if the slave is of the impedance-type. Position does not scale with orientation like it does with rectilinear motion; e.g. a full turn of the end effector is always 2π radians. For certain systems, it may be desirable to implement Pseudo-admittance control on the positioning stage of the robot, but another method for orientation.

Appendix: Linearizing and Decoupling Control

In this appendix we summarize the linearizing and decoupling control law as applied in this work. It is also known as the computed-torque method; details can be found in Craig (1989). A general serial-link robot is described by the dynamic equation

$$M(\Theta)\ddot{\Theta} + Q(\Theta, \dot{\Theta}) = \Upsilon_a + J^T(\Theta)F_{ext} \tag{69}$$

where Θ is the vector of generalized joint variables, $M(\Theta)$ is the positive-definite mass matrix, and $Q(\Theta, \dot{\Theta})$ is a vector containing Coriolis and centrifugal terms, as well as gravity effects and joint friction. The vector Υ_a represents the generalized joint actuator forces/torques, the vector F_{ext} represents the force that is externally applied to the end effector, and $J(\Theta)$ is the manipulator Jacobian mapping the joint velocities to the Cartesian velocity of the end-effector ($\dot{X} = J(\Theta)\dot{\Theta}$), expressed in the same frame as F_{ext}.

We can express the robot dynamics as a Cartesian robot of the form

$$M_x(\Theta)\ddot{X} + Q_x(\Theta, \dot{\Theta}) = F_a + F_{ext} \tag{70}$$

where F_a is the effective actuator force vector at the end-effector, which is related to the joint actuator forces/torques by

$$\Upsilon_a = J^T(\Theta)F_a. \tag{71}$$

The Cartesian matrices are constructed as

$$M_x(\Theta) = J^{-T}(\Theta)M(\Theta)J^{-1}(\Theta) \tag{72}$$

$$Q_x(\Theta, \dot{\Theta}) = J^{-T}(\Theta)(Q(\Theta, \dot{\Theta}) - M(\Theta)J^{-1}(\Theta)\dot{J}(\Theta)\dot{\Theta}). \tag{73}$$

Note this Cartesian formulation requires an invertible Jacobian; the Jacobian, when square, is invertible whenever the robot is not in a singular configuration.

A serial link Cartesian robot of (70) can be made to appear, to the controller, like a unit-mass linear and decoupled Cartesian robot:

$$\ddot{X} = F_c + M_x^{-1}(\Theta)F_{ext} \tag{74}$$

where F_c is the controller force that is designed assuming a linear and decoupled unit-mass robot. This is accomplished by applying an actuator force of the form:

$$F_a = M_x(\Theta)F_c + Q_x(\Theta, \dot{\Theta}). \tag{75}$$

Note that this linearizing and decoupling control law does not cancel the dynamics of the robot; this is evident from the presence of the Cartesian inertia matrix in (74). It does allow any additional controller to be designed for a unit-mass, decoupled system – that is, in (74), F_c controls $\ddot{X}$ directly in the absence of any external disturbances. The controller in (75) is idealized, and in practice we must use accurate estimates of M_x and Q_x.

Acknowledgment

This work is supported by National Science Foundation grants #ITR-0205318 and #IIS-0347464. The authors would like to thank Lawton Verner for his contributions towards the dual-PHANToM experimental setup, and Greg Hager for proposing this direction of research.

References

Abbott, J. J. (2005). *Virtual Fixtures for Bilateral Telemanipulation*. PhD Dissertation, Department of Mechanical Engineering, The Johns Hopkins University.

Abbott, J. J., Marayong, P., and Okamura, A. M. (2007). Haptic virtual fixtures for robot-assisted manipulation. *Robotics Research: Results of the 12th International Symposium ISRR (2005)*, pp. 49–64.

Abbott, J. J. and Okamura, A. M. (2003). Steady-hand teleoperation with virtual fixtures. *Proceedings of IEEE International Workshop on Robot and Human Interactive Communication (RO-MAN)*, pp. 145–151.

Abbott, J. J. and Okamura, A. M. (2006). Stable forbidden-region virtual fixtures for bilateral telemanipulation. *ASME Journal on Dynamic Systems, Measurement, and Control*, **128**(1): 53–64.

Adams, R. J. and Hannaford, B. (1999). Stable haptic interaction with virtual environments. *IEEE Transactions on Robotics and Automation*, **15**(3): 465–474.

Bettini, A., Marayong P., Lang, S., Okamura, A. M., and Hager, G. D. (2004). Vision-assisted control for manipulation using virtual fixtures. *IEEE Transactions on Robotics* **20**(6): 953–966.

Boctor, E., Webster, R. J. III, Mathieu, H., Okamura, A. M., and Fichtinger, G. (2004). Virtual remote center of motion control for needle placement robots. *Computer-aided Surgery*, **9**(5): 175–183.

Casals, A., Munoz, L., and Amat, J. 2003. Workspace deformation based teleoperation for the increase of movement precision. *Proceedings of IEEE International Conference on Robotics and Automation*, pp. 2824–2829.

Çavuşoğlu, M. C., Feygin, D., and Tendick, F. (2002). A critical study of the mechanical and electrical properties of the PHANToM haptic interface and improvements for high-performance control. *Presence*, 11(6): 555–568.

Colgate, J. E., Stanley, M. C., and Brown, J. M. (1995). Issues in the haptic display of tool use. *Proceedings of IEEE/RSJ International Conference on Intelligent Robots and Systems*, pp.140–145.

Craig, J. J., Hsu, P., and Sastry, S. S. (1987). Adaptive control of mechanical manipulators. *International Journal of Robotics Research*, **6**(2): 16–28.

Craig, J. J. (1989). *Introduction to Robotics: Mechanics and Control*, 2nd edn. Addison Wesley, Reading, MA.

Esen, H., Yano, K., and Buss, M. (2003). A control algorithm and preliminary user studies for a bone drilling medical training system. *Proceedings of IEEE International Workshop on Robot and Human Interactive Communication (RO-MAN)*, pp. 153–158.

Hashtrudi-Zaad, K. and Salcudean, S. E. (2001). Analysis of control architectures for teleoperation systems with impedance/admittance master and slave manipulators. *International Journal of Robotics Research*, **20**(6): 419–445.

Horn, R. and Johnson, C. R. (1985). *Matrix Analysis*. Cambridge University Press, Cambridge.

Kang, H. and Wen, J. T. (2000). Autonomous suturing using minimally invasive surgical robots. *Proceedings of IEEE International Conference on Robotics and Automation*, pp. 742–747.

Kim, W. S., Tendick, F., Ellis, S. R., and Stark, L. W. (1987). A comparison of position and rate control for telemanipulators with consideration of manipulator system dynamics. *IEEE Journal of Robotics and Automation*, RA-3(5): 426–436.

Kontz, M. E. and Book, W. J. (2003). Position/rate haptic control of a hydraulic forklift. *Proceedings of ASME International Mechanical Engineering Congress and Exposition*, pp. 801–808.

Lawrence, P. D., Salcudean, S. E., Sepehri, N., Chan, D., Bachmann, S., Parker, N., et al. (1995). Coordinated and force-feedback control of hydraulic excavators. *Lecture Notes in Control and Information Sciences, Vol. 223, 4th International Symposium on Experimental Robotics*, pp. 181–194, Springer-Verlag, London.

Micaelli, A., Bidard, C., and Andriot, C. 1998. Decoupling control based on virtual mechanisms for telemanipulation. In *Proc. IEEE International Conference Robotics and Automation*, pp. 1924–1931.

Mitra, P. and Niemeyer, G. (2004). Dynamic proxy objects in haptic simulations. In *Proceedings of IEEE International Conference on Robotics, Automation, and Mechatronics*, pp. 1054–1059.

Mobasser, F. and Hashtrudi-Zaad, K. (2004). Implementation of a rate mode impedance reflecting teleoperation controller on a haptic simulation system. *Proceedings of IEEE International Conference on Robotics and Automation*, pp. 1974–1979.

Moore, C. A., Peshkin, M. A., and Colgate, J. E. (2003). Cobot implementation of virtual paths and 3-D virtual surfaces. *IEEE Transactions on Robotics and Automation*, **19**(2): 347–351.

Parker, N. R., Salcudean, S. E., and Lawrence, P. D. (1993). Application of force feedback to heavy duty hydraulic machines. *Proceedings of IEEE International Conference on Robotics and Automation*, pp. 375–381.

Roy, J. and Whitcomb, L. L. (2002). Adaptive force control of position/velocity controlled robots: theory and experiment. *IEEE Transactions on Robotics and Automation*, **18**(2): 121–137.

Rugh, W. J. (1996). *Linear Systems Theory*, 2nd edn. Prentice-Hall, Upper Saddle River, NJ.

Ruspini, D. C., Kolarov, K., and Khatib, O. (1997). The haptic display of complex graphical environments. In *Proceedings of ACM International Conference on Computer Graphics and Interactive Techniques*, pp. 345–352.

Smid, M. (2000). In *Handbook of Computational Geometry* (eds J.-R. Sack and J. Urrutia), North Holland/Elsevier.

Tan, H. Z., Barbagli, F., Salisbury, K., Ho, C., and Spence, C. (2006). Force-direction discrimination is not influenced by reference force direction. *Haptics-e*, **4**(1): 1–6.

Turro, N., Khatib, O., and Coste-Maniere, E. (2001). Haptically augmented teleoperation. *Proceedings of IEEE International Conference on Robotics and Automation*, pp. 386–392.

Williams, R. L. II, Henry, J. M., Murphy, M. A., and Repperger, D. W. (1999). Naturally-transitioning rate-to-force control in free and constrained motion. *ASME Journal of Dynamic Systems, Measurement, and Control*, **121**(3): 425–432.

Zhai, S. and Milgram, P. (1993). Human performance evaluation of manipulation schemes in virtual environments. *Proceedings of First IEEE Virtual Reality Annual International Symposium*, pp. 155–161.

Zilles, C. B. and Salisbury, J. K. (1995). A constraint-based God-object method for haptic display. *Proceedings of IEEE/RSJ International Conference Intelligent Robots and Systems*, pp. 146–151.